Eur. Phys. J. B **41**, 325–332 (2004)
DOI: 10.1140/epjb/e2004-00325-4

THE EUROPEAN PHYSICAL JOURNAL B

Roles of interfaces in nanostructured silicon luminescence

C. Ternon, C. Dufour, F. Gourbilleau[a], and R. Rizk

SIFCOM, CNRS-UMR 6176, ENSICAEN 6 Boulevard Maréchal Juin, 14050 Caen Cedex, France

Received 6 April 2004
Published online 21 October 2004 –

Abstract. The increasing interest in photonics in the field of communication has led to intense research work on silicon based nanostructures showing efficient photoluminescence. The present paper reports photoluminescence measurements obtained at room temperature in silicon-rich-silica-silica multilayers grown by reactive magnetron sputtering. The silicon nanograin size is controlled via the silicon layer thickness which can be monitored with high accuracy. We aim to develop a comprehensive understanding of the combined roles played by the quantum confinement effect through the silicon grain size and the existence of an interfacial region between the grain and the surrounding silica matrix. Two bands of photoluminescence are displayed in the 600 nm–900 nm range and correspond to the bands previously observed at 2 K. Their origin is demonstrated through a model based on the solution of the Schrödinger equation of the exciton wavefunction in a one-dimension geometry corresponding to the growth direction of the multilayers. The silicon layer as well as the Si-SiO_2 interface thicknesses are the key parameters of the photoluminescence features.

PACS. 78.67.-n Optical properties of low-dimensional, mesoscopic, and nanoscale materials and structures – 73.21.Ac Multilayers – 71.23.An Theories and models; localized states

1 Introduction

The pioneering work of Canham on the efficient room temperature (RT) visible photoluminescence (PL) from porous silicon [1] has generated a tremendous research effort during the last decade. This has concerned single [2–4] and multilayered systems [5–8] of nanosized silicon showing remarkable optical properties, that contrast with poor optical feature of bulk silicon due to its narrow gap (1.12 eV at RT) and indirect interband transitions. The high energy (1.4−1.9 eV) PL emission observed from these systems was first attributed to the nanoscaled size of silicon through a quantum confinement effect [9,10] (QCE). Understanding of this phenomenon has been in constant development for a decade [11]. However, the experiments performed so far show some discrepancies with pure QCE. The most common structure leading to such a luminescence consists of silicon nanograins embedded in a transparent and insulating silica (SiO_2) matrix. Such structures present the combined advantages of compatibility with silicon technology, good mechanical robustness and chemical stability for potential applications. The main methods used to synthesize such Si-SiO_2 composite systems are: silicon ion implantation in thermally grown silica [12–17], plasma enhanced chemical vapor deposition (PECVD) [4,18–20] and magnetron cosputtering [2,21–23]. Photoluminescence studies reveal the existence of an emission peaking in the 1.2−1.7 eV range with a full width at half maximum (FWHM) of about 0.2 to 0.4 eV. While some authors point out the fact that the PL peak position is independent of the Si grain size [16,24], other workers reported a link between the PL peak and the grain size when it exceeds 3 nm [14,17]. The various luminescence features observed for the composite samples fabricated by different techniques might originate from the difficulty in controlling both size and distribution of the silicon nanograins within the host matrix. Such control was attempted through the deposition of Si/SiO_2 multilayers in which the thickness of the Si sublayer (<5 nm) is assumed to limit the size of the growing Si nanograins, as first reported by Lockwood et al. [9], who obtained efficient visible emission from samples deposited by molecular beam epitaxy (*MBE*). Apart from the expensive *MBE* technique, several processes have been developed beside the sputtering method to fabricate Si/SiO_2 multilayers such as PECVD [6] and reactive evaporation [25]. These experiments reported the detection of a unique large peak located between 1.3 and 2.3 eV, from crystallized or amorphous nanoscaled silicon, with a FWHM comparable to that of the single composite layers described above. Multilayered structures are attractive since the PL emission might be tuned through the silicon layer thickness that limits the size of the growing silicon nanograins.

[a] e-mail: fabrice.gourbilleau@ensicaen.fr

This paper aims at providing a correlation between the structure of the Si/SiO_2 multilayers and the corresponding PL properties in the 400−1800 nm (0.7−3.1 eV) range. The samples described below have been obtained by an original approach based on a newly developed reactive character of magnetron sputtering, briefly described in Section 2 and detailed in our previous work [26]. The peculiar two PL bands depicted in Section 3 have motivated the development of the model reported in Section 4 which shows the importance of both silicon sublayer thickness and Si/SiO_2 interfacial regions. The experimental and computational results are compared in Section 5 before being discussed in Section 6.

2 Experiment

The multilayers investigated in this study are fabricated by reactive magnetron sputtering from a unique pure silica target. During the deposition, the (100) Si substrate is maintained at 500 °C. The process consists in sputtering a silica target to deposit sequentially a silicon oxide layer under a pure argon plasma and a silicon-rich silica layer (SRSO) under a mixture of hydrogen and argon. These alternative depositions are repeated as many times as the planned periods. More details are given in previous work [26–28]. By modifying the deposition duration under the Ar/H_2 plasma, the thickness of the SRSO sublayer was controlled in the 0.6−3 nm range, while the silica layer thickness was maintained at 19 nm. The samples were then annealed at 1100 °C for 1 hour under a continuous flux of nitrogen. The microstructure was studied by high resolution electron microscopy (HREM) observations, while the light emitting properties were analysed by PL measurements using either several excitation lines from an argon laser (488 nm, 458 nm and 454 nm) or the 325 nm excitation line from a HeCd laser. The PL was detected by a Ag-O-Cs cathode photomultiplier (R5108) in the 400−1000 nm range and by nitrogen cooled Ge detector (Northcoast EO817) in the 800−1800 nm range.

3 Experimental evidence

We report hereafter the most relevant structural and optical features of our multilayers [29]. Figure 1 shows a typical TEM image of a multilayer with the corresponding electron diffraction pattern (EDP) for thickness of about 1.2 nm and 19 nm of SRSO and silica sublayers, respectively. The EDP (inset) displays a halo ring characteristic of amorphous material that explains the poor contrast displayed between SRSO and silica sublayers. The diffraction dots originate from the substrate observed along the [110] direction. Such an amorphous phase was found to form for all values of the SRSO sublayer thickness t_{Si} below 3 nm examined in this work and it contrasts with the crystallization observed for $t_{Si} > 3$ nm [28]. These results are in agreement with previous experimental studies which have shown that the crystallization of very thin silicon layers requires annealing temperatures higher than

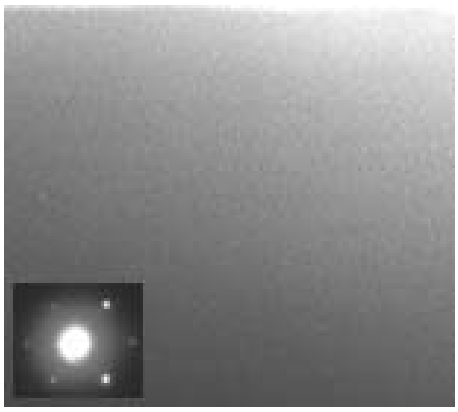

Fig. 1. TEM image of a multilayer with the corresponding electron diffraction pattern (EDP). Here the SRSO layer is about 1.2 nm and that of silica 19 nm. The EDP reveals that no crystalline material is present in the film. The diffraction dots originates from the substrate observed along the [110] direction.

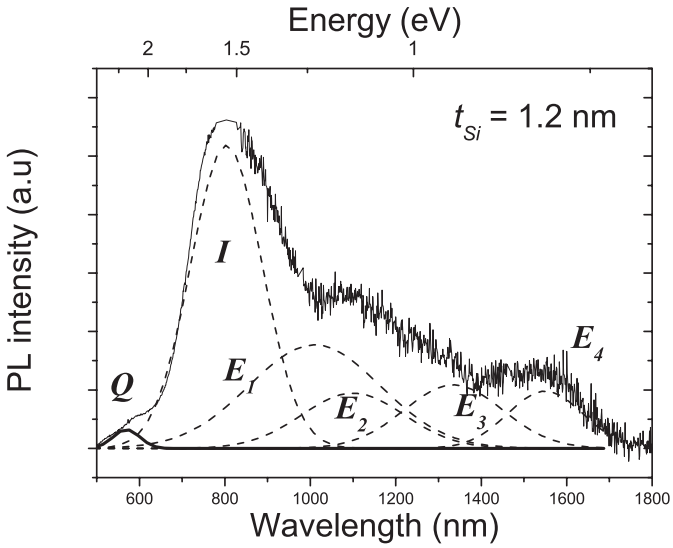

Fig. 2. PL spectrum at room temperature of a $SRSO/SiO_2$ multilayer with SRSO layer thickness of 1.2 nm. The dashed lines show the five Gaussian bands used to fit the spectrum.

1100 °C [30]. This fact was thermodynamically predicted by Veprek et al. [31] who showed that the silicon amorphous phase is stable when the grain size is smaller than 3 nm.

The typical PL spectrum corresponding to our multilayer with $t_{Si} < 3$ nm and recorded in the 500−1800 nm range is shown in Figure 2. We notice a lower signal to noise ratio in the 800−1700 nm range due to the detector change at 850 nm.

Six Gaussian bands were necessary to reproduce with a good accuracy the original spectrum. These bands labeled E_1, E_2, E_3 and E_4 are likely due to the transitions between localised states in the amorphous silicon bandgap, since their corresponding peak energies have

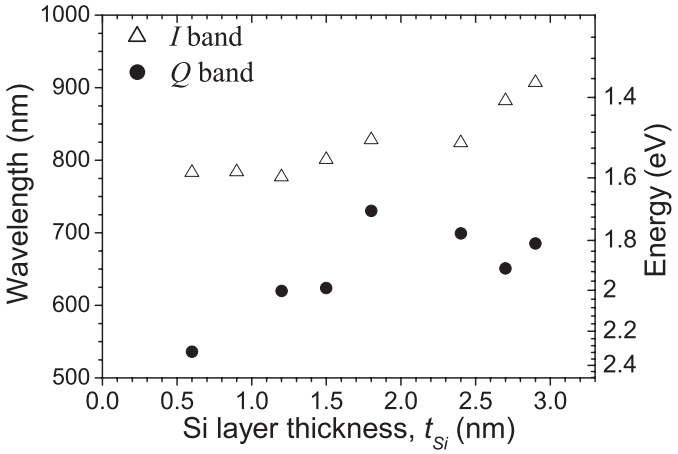

Fig. 3. PL peaks of Q and I bands as a function of the SRSO layer thickness.

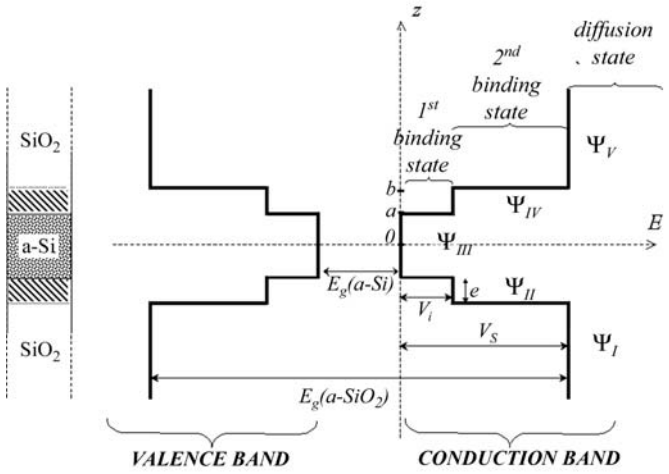

Fig. 4. Schematic representation of the finite square well with interface used to model one silicon layer sandwiched between two silica layers. For our convenience, the zero of energy is chosen at the bottom of the conduction band, so that the interfacial potential is V_i and that of silica V_S.

been found independent of the silicon layer thickness and agree well with the experimental values given by Street [32]: $E_1 = 1.23$ eV, $E_2 = 1.13$ eV, $E_3 = 0.93$ eV and $E_4 = 0.83$ eV. The two remaining bands, labeled I and Q, are located in the visible range and are dependent on the SRSO layer thickness. The evolution of the peak positions of these I and Q lines as a function of t_{Si} are shown in Figure 3.

To our knowledge, the present paper relates for the first time the observation at room temperature of both I and Q bands since they have only been seen at very low temperature (2 K) by Okamoto and Kanemitsu [33], who ascribed the I band to electron-hole recombination at the silicon/silica interface, and the Q band to quantum confinement in the silicon nanograins. More recently, a theoretical study [34] based on these experimental results has shown that the I and Q bands merge when some oxygen atoms are missing at the Si/SiO_2 interfacial region saturated with Si = O double bonds.

4 Model

The visible photoluminescence has been interpreted so far as resulting from the recombination of an electron-hole pair (exciton) either within a silicon nanograin [9,35] (quantum confinement), at the Si/SiO_2 interface [14,36] or at both grain and interface [37,38].

The model proposed in this study aims at the description of the concomitant behaviours of the two I and Q bands, assuming the following: (i) the silicon is amorphous as evidenced by TEM, (ii) the quantum confinement is effective and (iii) the interface plays a key role in the photoluminescence mechanism.

For our samples, the nanoscaled size concerns solely the growth direction (called z hereafter) in such a way that each silicon layer sandwiched between two silica layers acts as a unidimensional quantum well. In such structures, the excitons lie in a potential usually described by well functions [9,39]. Thus, the use of either finite [39] or infinite [9] square well potentials were not found satisfactory. The origin might lie in the non abrupt character of the Si/SiO_2 interface, as experimentally demonstrated [40,41]. This interfacial region, is indeed composed of suboxides, with a width that varies between 0.3 and 2.5 nm. We therefore suggest the use of the potential $V(z)$ depicted in Figure 4 with an energy origin located at the bottom of the conduction band. The half width of the well is characterized by the parameter a, the interfacial region by a width, e and an intermediate potential V_i, and finally the insulating barrier material by a potential V_S. The band gap of silicon and silica are respectively $E_g(a\text{-Si})$ and $E_g(SiO_2)$. Depending on the excitation energy E, such a geometry implies the coexistence of three states: (i) first binding state ($0 < E < V_i$), (ii) second binding state ($V_i < E < V_S$) and (iii) diffusion state ($E > V_S$).

For simplicity, we assume that any exciton generated within the system is associated with a specific pair of electron and hole subbands. This implies that the exciton binding energy is small compared to the energy band gaps of Si and SiO_2. According to previous work [42], this assumption is valid for quantum wells whose width is lower than 20 nm. We therefore calculate for each binding state, the PL transition energies from the lowest eigenvalues of the electrons and holes as well as the room temperature band gap, after neglecting the exciton energies. The highest excitation energy used is 3.8 eV so that the diffusion state is not taken into account, since it could only take place for excitation energies higher than $E_g(SiO_2)$.

The model is thus totally defined by the following parameters: the room temperature amorphous silicon band gap ($E_g(a\text{-Si})$), the insulating potential (V_S) which is directly related to the room temperature silica band gap through,

$$E_g(SiO_2) = 2V_s + E_g(a - Si), \quad (1)$$

the interfacial potential (V_i), the thickness of the interfacial region (e) and the effective mass of the exciton (m^*).

Within the approximation described above, the model has been developed from the one-dimensional Schrödinger equation for an electron-hole pair, as detailed in the Appendix.

5 Results

5.1 Luminescence energy

According to the calculation detailed in the Appendix, different expressions are determined for the two binding states in the four regions defined in the schematic diagram of Figure 4. The eigenenergy values corresponding to the first and second binding state are $\mathcal{E}_1$ and $\mathcal{E}_2$, respectively, and allowed the calculation of the PL transition energies from the relation $E_i^{PL} = E_g(a\text{-Si}) + \mathcal{E}_i$ where $i = 1, 2$ stands for the ith binding state.

The best fit between experimental data and calculated results, as shown in Figure 4, was obtained with the following values of the parameters:

- $E_g(a\text{-Si}) = 1.4$ eV: this value is very close to that of unhydrogenated amorphous silicon (1.5 eV at 295 K) [32].
- $V_s = 3.4$ eV: from this value, we deduce the silica band gap of 8.2 eV according to equation (1), in excellent agreement with the experimental value.
- $e = 0.8$ nm: this value lies exactly in the 0.3−2.5 nm range defined by experimental studies [40,41]. Moreover this value is consistent with the recent work of Daldosso et al. [43] in which they experimentally measured the interfacial region thickness (about 1 nm) and compared it to their calculated value (0.8–0.9 nm).
- $V_i = 0.3$ eV: a value that can be considered as a new data suggested by our model without any experimental counterpart previously reported.
- $m^* = 0.5m_e$ (free electron mass). This value is supported by two earlier studies: that of Lockwood et al. [9] for a-Si reports $m_e^* = m_h^* = m_e$ (i.e. $m^* = 0.5m_e$), while that of Barber et al. [44] states $m_e^* = 0.81m_e$ and $m_h^* = 1.18m_e$ for $c-$Si, leading to $m^* = 0.48m_e$.

According to Figure 5, the evolution of the experimental I band (open triangles) versus the silicon layer thickness is best fitted with the values calculated from the first binding state ($E < V_i$, continuous line) while that of the experimental Q band (black circles) is satisfactorily reproduced from the values obtained from the second binding state ($V_i < E < V_S$, dashed line). The model simulates satisfactorily the evolution of the I band wavelength versus the silicon layer thickness as well as the complex behaviour of the Q band wavelength. For this latter case, the discontinuity observed at $t_{\text{Si}} = 2$ nm is associated with the parity change of the states.

Even though no experimental data is available for $t_{\text{Si}} < 0.6$ nm, the model predicts a high energy shift of the Q band when t_{Si} is decreased.

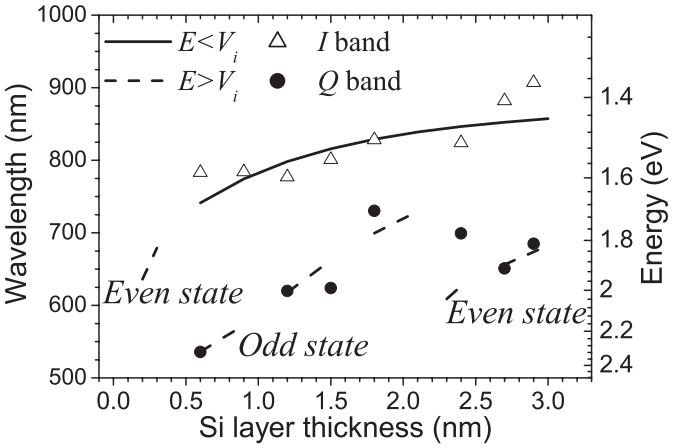

Fig. 5. Calculated PL transition energies as a function of the silicon layer thickness. The experimental data are plotted with triangles (I band) and circles (Q band).

5.2 Probability distribution function, $\mathcal{P}(z)$

The probability distribution function $\mathcal{P}(z)$ of the exciton is defined by $\mathcal{P}(z) = |\Psi(z)|^2$. From the various expressions (see Appendix) of the wavefunction $\Psi(z)$ in the first (Eqs. (A.6)) and in the second binding state (Eqs. (A.7)), $\mathcal{P}(z)$ was calculated and plotted against z in Figure 6. Figures 6a, b and c concern the eigenstates corresponding to $E < V_i$ (first binding state, I band) for three values of t_{Si} (0.3, 1.5 and 3 nm), respectively, while Figures 6a', b' and c' are their respective counterparts for the second binding state ($V_i < E < V_S$, Q band). All the remaining parameters are maintained constant with the same values reported in the previous Section 5.1.

The first binding state (linked to the I band) corresponds to an even solution of the Schrödinger equation (Eq. (A.1) in the Appendix). No solution is found for t_{Si} lower than 0.3 nm, whereas for higher t_{Si} values, $\mathcal{P}(z)$ indicates an exciton probability distribution function within the silicon layer: the value of $\int_{-a}^{a} \mathcal{P}(z)\,dz$ (hatched region) is higher than 1/2. The second binding state exists whatever the value of t_{Si}. For SRSO layer thicknesses lower than that of the interface thickness ($2e$), $\mathcal{P}(z)$ indicates that the exciton is most probably located at the Si/SiO_2 interface: $2\int_{a}^{a+e} \mathcal{P}(z)\,dz$ is higher than 1/2. With increasing t_{Si} values, the probability of finding the exciton within the silicon layers increases.

This study indicates that the eigenstate relating to the presence of an interfacial region is not necessary located within this region.

6 Discussion

Impact of the parameters

Our model involves the use of four parameters, (e, V_i, $E_g(a\text{-Si})$ and V_S, already defined, in addition to the

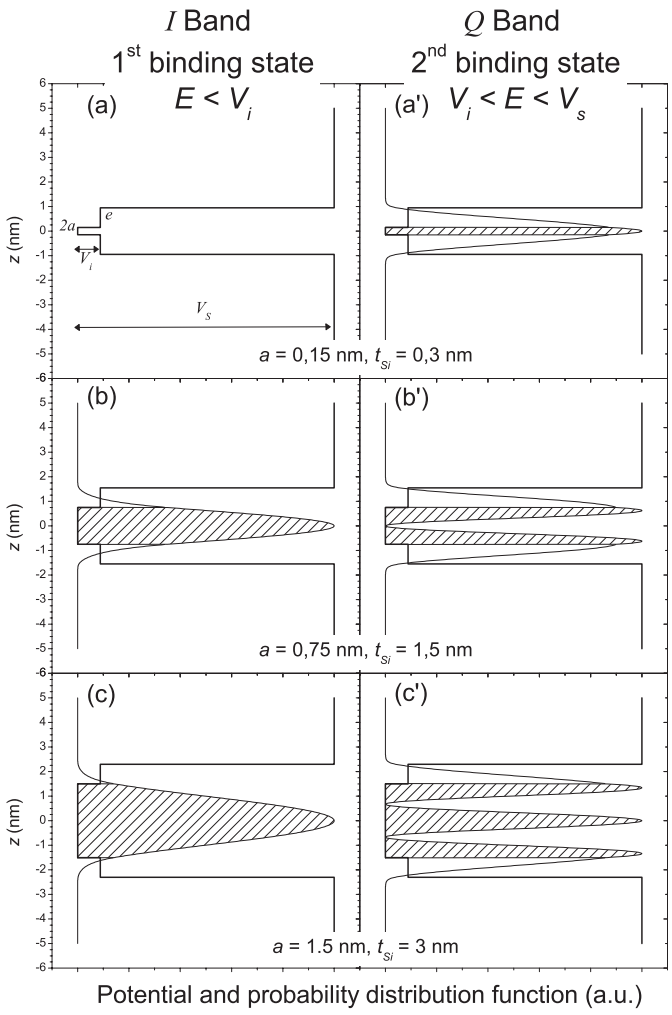

Fig. 6. Probability distribution function, $\mathcal{P}(z)$ (thin line) of the exciton in the well for various silicon layer thickness: 0.3, 1.5 and 3 nm for the two binding states. The potential profile (thick line) is also redrawn on each figure.

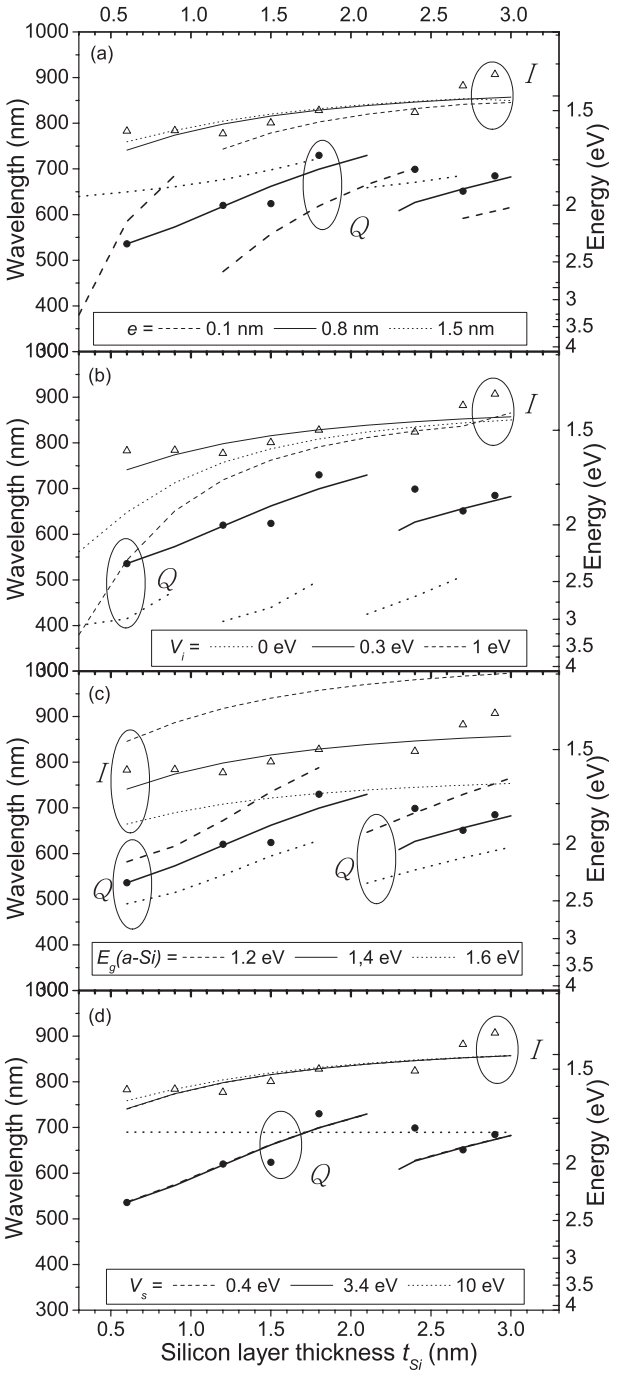

Fig. 7. Influence of each parameter (e, V_i, $E_g(a\text{-Si})$ and V_S) on the simultaneous behaviour of the I and Q bands as a function of the silicon layer thickness. The continuous line corresponds to the best fit of the experimental data (circles and triangles) whereas the dashed and dotted lines correspond to lower and upper values of the considered parameter.

effective exciton mass m^*). In this section, we investigate the influence of each parameter in order to show that only one set of values is able to provide a solution consistent with the experimental results. Figures 7a to d depict the effect of the parameters e, V_i, $E_g(a-\text{Si})$ and V_S, respectively, while the appropriate remaining parameters are fixed to the values corresponding to the best fits shown in Figure 5.

The I band is only slightly affected by the value of the interface thickness (e) whereas the Q band shows a noticeable change with e. Indeed, for high value of e (1.5 nm), the Q band is weakly dependent on t_{Si}, whereas, for low e values (0.1 nm), only one state is found (for $t_{\text{Si}} < 1.2$ nm). These two features disagree with the experimental measurements.

Neglecting the interfacial potential ($V_i \to 0$), we deal with a finite square well giving rise to a unique emission band instead of the two bands (I and Q) experimentally detected. The emergence of V_i favors the detection of the second band Q, which shifts towards high energies for increasing V_i values. Besides, the I band energy is radically modified for the smaller values of t_{Si}.

The investigation of $E_g(a\text{-Si})$ shows that the variation of this parameter leads to an overall global energy shift of both bands. Finally the insulating potential, V_S, does not

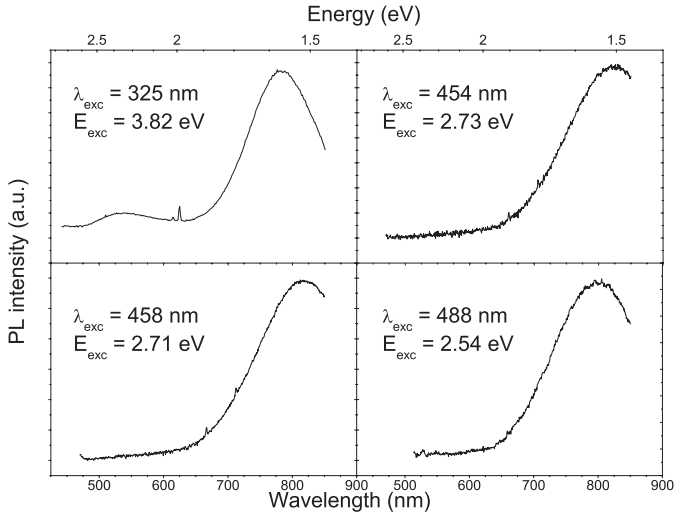

Fig. 8. Excitation energy effect on the emission of a multilayer with $t_{\mathrm{Si}} = 0.6$ nm.

affect the behavior of I band, but low values (<1.2 eV) induce radical change for Q.

According to the calculations, this latter emission band can be present only for excitation energies higher than the critical value deduced from: $E_{exc}^{lim} = E_g(a\text{-Si}) + 2 * V_i = 2.0$ eV. We have experimentally verified this assumption by performing photoluminescence measurements with different excitation lines from an argon and He-Cd lasers. Figure 8 shows the corresponding photoluminescence spectra recorded in the case of multilayer with $t_{\mathrm{Si}} = 0.6$ nm. The same characteristic has been noticed for higher values of t_{Si} up to 1.6 nm.

The Q band appears only for the highest (3.82 eV) excitation energy used. The excitation threshold is apparently located in the 2.73−3.82 eV range which does not contain the value of 2.0 eV deduced from the modeling. However it has been demonstrated [45] that, depending on fabrication conditions, the Stokes shift in silicon can reach a value as high as 0.6 eV. Considering the uncertainty relating to both theoretical and experimental approaches, the conjunction of the Stokes shift and 10% uncertainty can account for the fair agreement between calculated and experimental excitation values. The existence of the I band is predicted by this calculation and its near insensitivity toward the silicon layer thickness, is mainly due to the presence of an interfacial silicon/silica region. Moreover, its energy is straightforwardly governed by the value of the amorphous silicon band gap $E_g(a\text{-Si})$.

7 Conclusion

The photoluminescence features of Si/SiO_2 multilayers examined in this work appears closely governed by the silicon sublayer thickness varying between 0.6 and 3 nm. They concern the two coexisting visible emissions in addition to the well-known four infrared bands from amorphous silicon. These two visible bands have already been observed [33] but at low temperature (2 K) by Okamoto and Kanemitsu. In our films, these bands have been easily observed at 300 K. As proposed by several theoretical studies [34,43], the quantum confinement in the nanostructures and the Si/SiO_2 interfacial region are two conceivable candidates to explain the photoluminescence properties, but it is difficult to confirm this experimentally. However, the evolution versus SRSO layer thickness is not in agreement with previous theoretical work. As a consequence we have developed a model based on quantum wells. Our aim was to emphasize the physics underlying the emission phenomenon. In this way we have demonstrated that the coexistence of two emission bands in the visible region, one located at about 1.44 eV (800 nm) and the second tunable with the silicon layer thickness, were sensitive to the presence of an interfacial region between silicon and silica. Thus, through our experimental and theoretical work on nanosized amorphous silicon, the results obtained coincide with the previous conclusions of Degoli and Ossicini [34] and Daldosso et al. [43] concerning silicon nanocrystals: the interfacial region between silicon and silica plays a key role in the optical properties of nanosized silicon, whatever the phase, amorphous or crystalline.

The authors wish to thank Christophe Delerue for useful discussion. Céline Ternon acknowledges the Region Basse Normandie for financial support.

Appendix

Our aim is to solve the Schrödinger equation given by:

$$-\frac{\hbar^2}{2m^*}\,\frac{\partial^2\Psi(z)}{\partial z^2} + V(z)\Psi(z) = \mathcal{E}\,\Psi(z) \qquad \text{(A.1)}$$

where m^* is the reduced mass of the exciton, a function of the electron and hole effective masses,

$$\frac{1}{m^*} = \frac{1}{m_e^*} + \frac{1}{m_h^*} \qquad \text{(A.2)}$$

$\Psi(z)$ the one-dimensional exciton wavefunction and $V(z)$ the confining potential depending on z as shown in Figure 4:

$$\begin{cases} \text{if } z \in [-a, a], & \text{then } V(z) = 0, \\ \text{if } z \in [-b, -a] \cup [a, b], & \text{then } V(z) = V_i, \\ \text{if } z < -b \text{ and } z > b, & \text{then } V(z) = V_s. \end{cases}$$

The boundary conditions allowing the complete resolution of the problem are: (i) continuity of $\Psi(z)$ at the interfaces ($z = \pm a$ and $z = \pm b$); (ii) continuity of the derivative $\dfrac{\partial\Psi}{\partial z}$ at the interfaces ($z = \pm a$ and $z = \pm b$) and (iii) Ψ tends toward 0 for $z \to \infty$. Considering the symmetry of $V(z)$, the eigenstates are completely determined by solving the equation for $z > 0$, leading to the

following expressions for Ψ in the different regions:

$$\begin{cases} \text{Region } III \ z \in [-a,a], \\ \qquad\qquad \Psi(z) = A\cos kz \quad \text{(even)} \\ \qquad\qquad \Psi(z) = B\sin kz \quad \text{(odd)} \\ \text{Region } IV \ z \in [a,b], \\ \qquad\qquad \Psi(z) = Ce^{-qz} + De^{+qz} \\ \text{Region } V \quad z > b, \Psi(z) = Ge^{-pz}. \end{cases}$$

The constants A, B, C, D are replaced with their accurate expressions in the following lines while G is determined by the normalisation of the wavefunction.

The permitted wavevectors k are deduced from the following transcendental equations:

$$\begin{cases} ka\tan ka = \dfrac{pa\cosh qe + qa\sinh qe}{\cosh qe + \frac{p}{q}\sinh qe} \\ \qquad\qquad \textit{(even states)} \qquad \text{(A.3)} \\ \dfrac{\tan ka}{ka} = -\dfrac{\cosh qe + \frac{p}{q}\sinh qe}{pa\cosh qe + qa\sinh qe} \\ \qquad\qquad \textit{(odd states)} \qquad \text{(A.4)} \end{cases}$$

where $q^2 = \left|\dfrac{2m^*V_i}{\hbar^2} - k^2\right|$ and $p^2 = \left|\dfrac{2m^*V_s}{\hbar^2} - k^2\right|$. The eigenvalues of the particles are:

$$\mathcal{E} = \frac{\hbar^2k^2}{2m^*}. \qquad \text{(A.5)}$$

The first binding state is associated to the following wavefunction:

$$\begin{cases} \Psi_{III}^{even} = G\dfrac{q\cosh qe + p\sinh qe}{q\cos ka}e^{-pb}\cos kz & \text{(A.6a)} \\ \Psi_{III}^{odd} = G\dfrac{q\cosh qe + p\sinh qe}{q\sin ka}e^{-pb}\sin kz & \text{(A.6b)} \\ \Psi_{IV} = G\dfrac{q-p}{2q}e^{-(q+p)b}e^{qz} + \dfrac{q+p}{2q}e^{-(p-q)b}e^{-qz} & \text{(A.6c)} \\ \Psi_V = Ge^{-pz} & \text{(A.6d)} \end{cases}$$

while the second binding state is described by:

$$\begin{cases} \Psi_{III}^{'even} = G'\dfrac{q\cos qe + p\sin qe}{q\cos ka}e^{-pb}\cos kz & \text{(A.7a)} \\ \Psi_{III}^{'odd} = G'\dfrac{q\cos qe + p\sin qe}{q'\sin ka}e^{-pb}\sin kz & \text{(A.7b)} \\ \Psi'_{IV} = G'\left(\cos q(z-b) + \dfrac{p}{q}\sin q(z-b)\right)e^{-pb} & \text{(A.7c)} \\ \Psi'_V = G'e^{-pz} & \text{(A.7d)} \end{cases}$$

where G and G' are normalisation coefficients.

References

1. L.T. Canham, Appl. Phys. Lett. **57**, 1046 (1990)
2. S. Charvet, R. Madelon, F. Gourbilleau, R. Rizk, J. Lumin. **80**, 257 (1999)
3. B. Garrido, M. Lopez, C. Garcia, A. Perez-Rodriguez, J.R. Morante, C. Bonafos, M. Carrada, A. Claverie, J. Appl. Phys. **91**, 798 (2002)
4. T. Inokuma, Y. Wakayama, T. Muramoto, R. Aoki, Y. Kurata, S. Hasegawa, J. Appl. Phys. **83**, 2228 (1998)
5. M. Benyoucef, M. Kuball, J.M. Sun, G.Z. Zhong, X.W. Fan, J. Appl. Phys. **89**, 7903 (2001)
6. V. Vinciguerra, G. Franzo, F. Priolo, F. Iacona, C. Spinella, J. Appl. Phys. **87**, 8165 (2000)
7. Z.H. Lu, D.J. Lockwood, J.M. Baribeau, Nature **378**, 258 (1995)
8. P. Photopoulous, A.G. Nassiopoulou, D.N. Kouvatsos, A. Travlos, Appl. Phys. Lett. **76**, 3588 (2000)
9. D.J. Lockwood, Z.H. Lu, J.M. Baribeau, Phys. Rev. Lett. **76**, 539 (1996)
10. X.L. Wu, G.G. Siu, S. Tong, X.N. Liu, F. Yan, S.S. Jiang, X.K. Zhang, D. Feng, Appl. Phys. Lett. **69**, 523 (1996)
11. O. Bisi, S. Ossicini, L. Pavesi, Surf. Sci. Rep. **38**, 1 (2000)
12. L. Rebohle, J. Von Borany, R.A. Yankov, W. Skorupa, I.E. Tyschenko, H. Fröb, K. Leo, Appl. Phys. Lett. **69**, 523 (1996)
13. L.S. Liao, X.M. Bao, X.Q. Zheng, N.S. Li, N.B. Min, Appl. Phys. Lett. **68**, 850 (1996)
14. T.S. Iwayama, N. Kurumado, D.E. Hole, D. Towsend, J. Appl. Phys. **83**, 6018 (1998)
15. M.L. Brongersma, P.G. Kik, A. Polman, K.S. Min, H.A. Atwater, Appl. Phys. Lett. **76**, 351 (2000)
16. L. Pavesi, L. Dal Negro, C. Mazzoleni, G. Franzo, F. Priolo, Nature **408**, 440 (2000)
17. B. Garrido, M. Lopez, O. Gonzalez, A. Perez-Rodriguez, J.R. Morante, Appl. Phys. Lett. **77**, 3143 (2000)
18. A.J. Kenyon, P.F. Trwoga, C.W. Pitt, J. Appl. Phys. **79**, 9291 (1996)
19. F. Iacona, G. Franzo, C. Spinella, J. Appl. Phys. **87**, 1295 (2000)
20. X. Wu, A.M. Bittner, K. Kern, Ch. Eggs, S. Veprek, Appl. Phys. Lett. **77**, 645 (2000)
21. Q. Zhang, S.C. Bayliss, D.A. Hutt, Appl. Phys. Lett. **66**, 1977 (1995)
22. Y. Kansagawa, T. Kageyama, S. Takeoka, M. Fugiti, S. Hayashi, Y. Yamamoto, Solid State Commun. **102**, 533 (1997)
23. S. Takeoka, M. Fujii, S. Hayashi, Phys. Rev. B **62**, 16820 (2000)
24. Y. Kanemitsu, N. Shimizu, T. Komoda, P. Hemment, B. Sealy, Phys. Rev. B **54**, R14329 (1996)
25. M. Zacharias, J. Heitmann, R. Scholz, U. Kahler, M. Schmidt, J. Bläsing, Appl. Phys. Lett. **80**, 661 (2002)
26. C. Ternon, F. Gourbilleau, C. Dufour, J.L. Doualan, B. Garrido, J. Lumin. **99**, 361 (2002)
27. C. Ternon, F. Gourbilleau, X. Portier, P. Voivenel, C. Dufour, Thin Solid Films **419**, 5 (2002)
28. F. Gourbilleau, X. Portier, C. Ternon, P. Voivenel, R. Madelon, R. Rizk, Appl. Phys. Lett. **78**, 3058 (2001)
29. C. Ternon, F. Gourbilleau, R. Rizk, C. Dufour, Phys. E **16**, 517 (2003)
30. M. Zacharias, J. Bläsing, P. Veit, L. Tsybeskov, K. Hirschman, P.M. Fauchet, Appl. Phys. Lett. **74**, 2614 (1999)
31. S. Veprek, Z. Iqbal, F.A. Sarott, Phil. Mag. B **45**, 137 (1981)

32. R.A. Street, Adv. Phys. **25**, 397 (1976)
33. S. Okamoto, Y. Kanemitsu, Solid State Commun. **103**, 573 (1997)
34. E. Degoli, S. Ossicini, Surf. Sci. **470**, 32 (2000)
35. C. Delerue, G. Allan, M. Lannoo, Phys. Rev. B **48**, 11024 (1993)
36. Y. Kanemitsu, T. Ogawa, K. Shiraishi, K. Takeda, Phys. Rev. B **48**, 4883 (1993)
37. F. Koch, V. Petrova-Koch, T. Muschik, A. Nikolov, V. Gavrilenko, Mat. Res. Soc. Symp. Proc. **283**, 197 (1993)
38. M.V. Wolkin, J. Jorne, P.M. Fauchet, G. Allan, C. Delerue, Phys. Rev. Lett. **82**, 197 (1999)
39. S.B. Zhang, C.Y. Yeh, A. Zunger, Phys. Rev. B **48**, 11204 (1993)
40. N. Awaji, S. Ohkubo, T. Nakanishi, T. Aoyama, Y. Sugita, K. Takasaki, S. Komiya, Appl. Phys. Lett. **71**, 1954 (1997)
41. Y.P. Kim, S.K. Choi, H.K. Kim, D.W. Moon, Appl. Phys. Lett. **71**, 3504 (1997)
42. R.P. Leavitt, J.W. Little, Phys. Rev. B **42**, 11774 (1990)
43. N. Daldosso, M. Luppi, S. Ossicini, E. Degoli, R. Magri, G. Dalba, P. Fornasini, R. Grisenti, F. Rocca, L. Pavesi, S. Boninelli, F. Priolo, C. Spinella, F. Iacona, Phys. Rev. B **68**, 085327 (2003)
44. H.D. Barber, Solid State Electron. **10**, 1039 (1967)
45. R.A. Street, J.C. Knights, D.K. Biegelsen, Phys. Rev. B **18**, 1880 (1978)